

# Efficient Optical Trapping and Visualization of Silver Nanoparticles

Lana Bosanac, Thomas Aabo, Poul M. Bendix, and Lene B. Oddershede\*

*Niels Bohr Institute, University of Copenhagen, Blegdamsvej 17, 2100 Copenhagen, Denmark*

*Received February 19, 2008; Revised Manuscript Received March 14, 2008*

## ABSTRACT

We performed efficient optical trapping combined with sensitive optical detection of individual silver nanoparticles. The particles ranging in size from 20 to 275 nm in diameter were trapped in three dimensions using low laser power by minimizing spherical aberrations at the focus. The optical forces were quantified, and we found that the larger the particle, the stronger the optical force. The particles were imaged by an additional strongly scattered laser.

Silver and gold nanoparticles have since ancient times been utilized to color glass. Also, they have been used for medical purposes due to their antimicrobial properties and are very efficient as probes for nanotechniques. To some extent, the physical and chemical properties of silver nanoparticles are comparable to gold. However, use of gold nanoparticles in conjunction with fluorescent techniques is complicated by the fact that the absorption spectrum of gold nanoparticles peaks in the visible range where most fluorophores emit light. Hence, gold nanoparticles severely quench fluorescence. Silver nanoparticles absorb much less light in the visible spectrum and consequently do not quench conjugated fluorescent molecules nearly to the same extent. In fact, silver nanoparticles are known to enhance the fluorescent yield of certain fluorophores.<sup>1</sup> This makes silver nanoparticles an obvious choice as nanomarkers and handles in, e.g., biological samples, which are also fluorescently labeled. Until now, less effort has been put into, e.g., chemical conjugation or optical visualization and manipulation of silver nanoparticles in comparison to gold. However, we foresee that they will become increasingly used as probes in nanocircuits and environments.

Optical trapping using a single laser beam in three dimensions of 36 nm gold nanoparticles was first reported in 1994.<sup>2</sup> Later, optical trapping range of gold nanoparticles has been expanded to particles ranging from 18 to 254 nm in diameter.<sup>3</sup> Much less effort has been put into optical control of silver nanoparticles. Optical control of silver nanoparticles has been theoretically proposed,<sup>4</sup> and they have been reported to be optically trapped in two dimensions.<sup>5</sup> To our knowledge, silver nanoparticles have not previously been reported individually optically trapped in three dimen-

sions. Aggregates of silver nanoparticles have been optically trapped in 3D in order to perform local electric field enhancements with the goal of creating surface-enhanced hyper-Raman spectroscopy.<sup>6</sup>

In the present letter, we demonstrate three-dimensional optical trapping combined with efficient detection of single silver metallic nanoparticles. We quantify optical trapping constants for Rayleigh silver nanoparticles of various sizes by using an infrared CW laser with a wavelength of 1064 nm. There are several reasons for choosing this wavelength, the most important being that it is far above the plasmon resonance wavelength,<sup>5</sup> thus decreasing the destabilizing scattering and absorption forces. Also, this is a commonly used wavelength for optical trapping due to this wavelength's low absorptivity in biological material and low degree of optical damage on biological specimen. Optical trapping of metallic nanoparticles has been proposed to be associated with a significant heating of the particles caused by absorption of light.<sup>7</sup> This possible heating is a potential problem for biological use of optically trapped metallic particles. However, we used a newly developed method that significantly increases the efficiency of optical trapping by compensating spherical aberrations.<sup>8</sup> Hence, very low laser powers were used and the heating correspondingly reduced. This improved method allowed us to perform stable optical trapping of individual silver nanoparticles with diameters ranging from 20 to 275 nm. We found no upper bound for the particle sizes which could be trapped. The investigated size range was limited by the commercial availability of particles. We have performed a quantitative analysis of the optical forces in three dimensions exerted on the silver nanoparticles; the larger the particle, the larger the optical force exerted. Simultaneous trapping and imaging was accomplished by illuminating the particle with blue light,

\* Corresponding author. E-mail: oddershede@nbi.dk. Telephone: 45 35325287. Fax: 45 35325425.

which was strongly scattered by the surface plasmons of the particle. The infrared laser used for trapping was coupled into a commercially available microscope, which can be operated in confocal reflection mode, yielding a bright and nonfading signal of the trapped particle. We also visualized nanoparticles adsorbed to a glass substrate and found that the reflected intensity was strongly size dependent and exhibited a change in contrast relative to the background for increasing particle sizes, similar to what has been reported for gold nanoparticles.<sup>9,10</sup>

We purchased silver nanoparticles with diameters 20, 40, 60, 80, 100, 142, 168, 225, and 275 nm, the standard deviation of the diameters being  $\sim 10\%$ . Particles with diameters 20–80 nm were bought from BBI International, those with diameters 100–275 from Nanocomposix. The silver colloids were ultrasonicated for 30 s to break possible agglomerates and afterward stabilized with thiolated PEG in order to prevent them from aggregating. The thickness of the PEG coating was negligible in comparison to the diameter of the particles and had no influence on their trapping capabilities. The PEG stabilized colloids were diluted in deionized water until reaching a dilution where there was a minimum waiting time of  $>2$  min for a bead to diffuse into the trap. This was to reduce the risk of having multiple beads in the trap simultaneously, which was a likely situation that would change, e.g., the appearance of the power spectrum. The effect of optical binding can produce stable configurations of multiple nanoparticles in the trap.<sup>11</sup>

The colloid solution was flushed into a perfusion chamber consisting of two layers of glass cover slips, thickness 0.15 mm, separated and sealed by vacuum grease. For confocal visualization of the silver nanoparticles, the procedure was as described above, but in addition, 30 mM NaCl was added to the sample to make the silver nanoparticles attach firmly to the glass cover slip.

The optical trap used for quantitative measurements of the optical forces was implemented in an inverted Leica microscope (Leica DMIRB HC) equipped with a quadrant photodiode (S5981, Hamamatsu) for 3D position detection.<sup>12</sup> The trapping laser (Spectra Physics Millennia, 10 W) had a wavelength of 1064 nm. The objectives used were a  $100\times$  water immersion objective (Leica, PL APO, NA = 1.2) and a  $63\times$  oil immersion objective (Leica, HCX PL APO, NA = 1.32). To minimize spherical aberrations and hence produce the most efficient optical trap, an immersion oil with a refractive index of 1.54 was used for trapping in connection with the oil immersion objective, which creates optimal conditions while trapping the particle at a height of  $5\ \mu\text{m}$  from the inner surface of the chamber.<sup>8</sup> The voltage signal from the quadrant photodiode was detected and processed by custom-made Labview programs. These programs had an online calibration procedure, and the appearance of the power spectrum gave information of whether a particle was in the trap. The laser power at the sample necessary for trapping a particle depended somewhat on the particle size and ranged from 0.05 to 0.30 W.

The confocal visualization was performed using a Leica SP5 confocal microscope in reflection mode (using the 488

nm Ar line). In all pictures, the zoom was the same but the gain and pinhole were adjusted to get the largest contrast in the picture. Another laser trap, based on a Spectra 5 W 1064 nm laser, was implemented in the confocal microscope,<sup>13</sup> and this combination was used to take a picture of a trapped particle (as shown in Figure 6).

The optical forces acting on an optically trapped metallic Rayleigh particle are the absorption force, the scattering force, and the gradient force. Expressions for these forces are given, e.g., in ref 3. To achieve successful trapping, the gradient force must exceed the sum of the others. The forces are given by

$$F_{\text{grad}} = \frac{|\alpha|}{2} \nabla \langle E^2 \rangle \quad (1)$$

$$F_{\text{scat}} = \frac{n}{c} \langle P \rangle C_{\text{scat}} \quad (2)$$

$$F_{\text{abs}} = \frac{n}{c} \langle P \rangle C_{\text{abs}} \quad (3)$$

where  $E$  is the electrical field,  $n$  is the index of refraction of the surrounding media,  $P$  is the Poynting vector, and  $C_{\text{scat}}$  and  $C_{\text{abs}}$  denote the scattering and absorption cross sections of the particle.  $\alpha$  is the polarizability of the particle given by the Clausius–Mossotti relation  $\alpha = \alpha' + i\alpha'' = 3V(\epsilon_{\text{Ag}} - \epsilon_w)/(\epsilon_{\text{Ag}} + 2\epsilon_w)$ . Here,  $\epsilon_w$  and  $\lambda = 1064$  nm, and  $V$  is the volume of the particle.  $C_{\text{scat}}$  and  $C_{\text{abs}}$  are functions of  $\alpha$ .

To apply the Clausius–Mossotti relation to particles with radii  $r \geq \delta$ , where  $\delta$  is the skin depth of silver ( $\delta = 23.5$  at 1064 nm), one has to correct for the attenuation of the field inside the particle. The dielectric function of silver is a complex number,  $\epsilon_{\text{Ag}} = \epsilon' + i\epsilon'' = -52 + i3.397$ , the real part describing the refraction and the imaginary part describing the absorption of light in the silver. Hence, the gradient force is proportional to the polarized volume of the trapped particle. If the particle has a radius much smaller than the skin depth, the particle becomes uniformly polarized and the gradient force can be assumed to be proportional to the volume of the particle. However, for larger particles, the electric field only partially penetrates the particle and the gradient force increases more slowly than the volume of the particle. As written in eqs 2 and 3,  $F_{\text{scat}}$  and  $F_{\text{abs}}$  are proportional to the scattering and absorption cross sections, respectively. At the plasmon resonance of silver nanoparticles, the polarizability rapidly increases.<sup>14</sup>  $F_{\text{grad}}$  scales with polarizability and  $F_{\text{scat}}$  scales with polarizability squared. Thus, at wavelengths close to the plasmon resonance, the gradient force does not exceed the scattering force and trapping is probably not possible. However, the infrared laser light used in this study is far away from the plasmon resonance of silver, and the scattering and absorption cross sections at this wavelength are small enough that the gradient force can overcome the scattering and absorption forces.

Because of the Gaussian focal intensity distribution, we can express the gradient force given in eq 1 as a harmonic restoring force acting on the particle,  $F = -k(x-x_0)$ , where  $k$  is the spring constant describing the stiffness of the potential,  $x$  is the position of the particle, and  $x_0$  denotes its equilibrium position. This is true in all three dimensions, however, with different spring constants in each dimension.

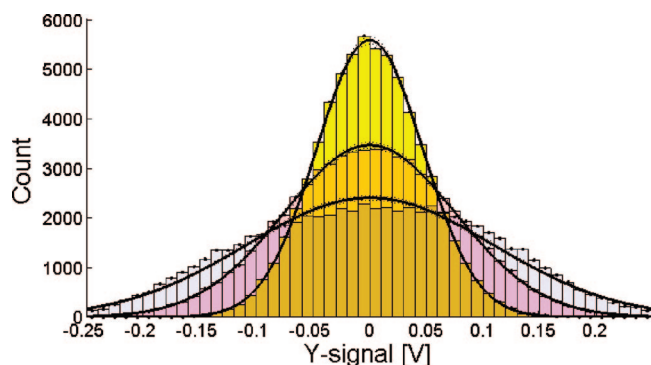


**Figure 1.** Three position histograms of nonoverlapping parts of the same time series with an increasing number of particles in the trap for each histogram.

Typically, for large particles such as micrometer-sized polystyrene beads, the spring constants perpendicular to the propagation direction of the trapping laser are nearly identical and the spring constant describing the potential in the axial direction is approximately half of those. However, for smaller particles this changes, and the spring constants in the perpendicular directions become dependent on whether they are along or orthogonal to the polarization direction of the laser light.<sup>15</sup> Also, by using the oil immersion objective and optimizing the immersion oil refractive index,<sup>8</sup> the axial spring constant can be made nearly as strong as the lateral directions. In our experiments,  $k$  was found in all three dimensions by monitoring the Brownian motion of an optically trapped particle. A Fourier analysis of each time series yielded a power spectrum that was well fitted by a Lorentzian function with a characteristic corner frequency given by  $f_c = \kappa/2\pi\gamma$ . Here,  $\gamma = 3\pi\eta d$  is the drag coefficient for a particle suspended in a fluid with viscosity  $\eta$ . The size of the particle was small enough in comparison to the distance to any surfaces that corrections to Stokes law, due to surface effects, could be neglected.

To perform the calibration, we used the programs described in ref 16, this program corrected for the pronounced filtering effect of the quadrant photodiode.<sup>17</sup> While measuring the time series of the excursions of the trapped particle in the directions orthogonal to the propagation of the laser light, the iris at the condenser of the microscope was fully opened. However, to get the largest sensitivity in the axial direction, the condenser was partially closed.<sup>18</sup> The time series were taken with a sampling frequency of 22 kHz.

We detected the presence of a trapped particle by an online processing of the measured time series. If the power spectrum of the time series was well fit by a Lorentzian function, and if the signal was well above that of an empty trap, most likely at least one silver nanoparticle was trapped. As the optical trap is exerting a harmonic potential on the trapped particle, the position distribution is well described by a Gaussian distribution, the width of the distribution being indicative of the number of particles in the trap.<sup>3</sup> Figure 1 shows position histograms of three nonoverlapping parts of the same time series. In the beginning, probably only a single particle was trapped, and the distribution is fairly narrow. After a couple of minutes, the histogram broadens, probably because

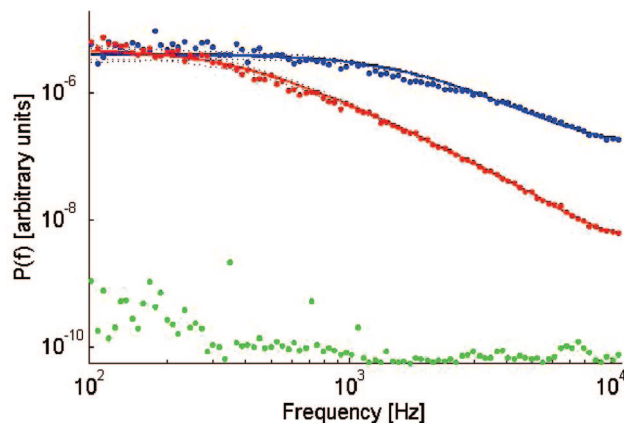


**Figure 2.** Power spectra recorded from optically trapped silver nanoparticles having diameters 60 nm (red) and 275 nm (blue). Full lines show Lorentzian fits to data. The power spectrum from an empty trap is shown for comparison (green).

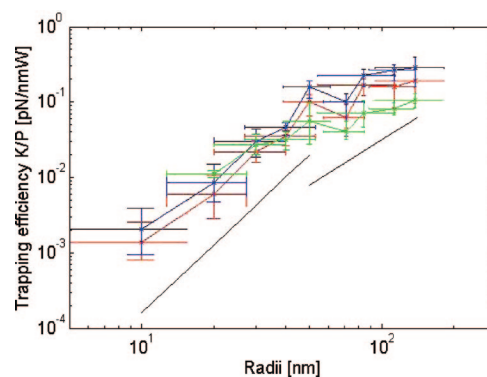


**Figure 3.** Data from optical trapping of individual silver nanoparticles using a water immersion objective. Spring constant,  $k$ , normalized by laser power, is shown as a function of particle radius. Data for all three independent translational directions,  $k_x$  (red),  $k_y$  (blue), and  $k_z$  (green) are shown. Black lines with slopes of 2 and 3 are drawn for comparison.

a second particle entered the trap. The broadest histogram is from a part of the time series where at least three particles were in the trap.

Figure 2 shows power spectra from optically trapped 60 and 275 nm silver nanoparticles using laser powers of 0.05 and 0.10 W measured at the sample. For comparison, the power spectrum from an empty trap is also shown. The signal from a nonempty trap is  $\sim 4$  orders of magnitude above that of an empty trap. The full lines are fits to the data by Lorentzian functions.

To quantify the strength of the optical trap for various particle sizes, we found the trap stiffness,  $k$ , in the lateral ( $x$ ,  $y$ ) and axial ( $z$ ) directions while trapping a single particle. Different sizes of particles required different laser powers for successful optical trapping. The trap stiffness is directly proportional to the laser power. To compare the data obtained for different particle sizes and different laser powers, we considered the normalized trap stiffness ( $k$  divided by laser power at the sample). Figure 3 shows the normalized trap stiffness as a function of particle radius using a water immersion objective. The error bar on particle size is given by the manufacturer.

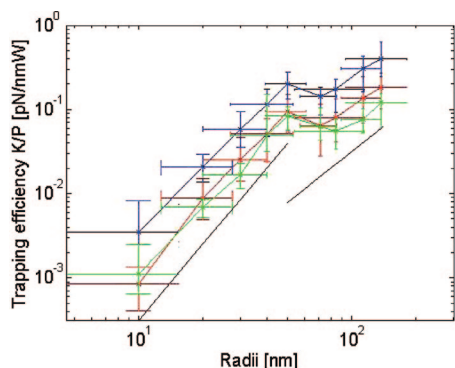


**Figure 4.** Data from optical trapping of individual silver nanoparticles using an oil immersion objective with optimized immersion media. Normalized spring constant,  $k$ , is shown as a function of particle radius. Data for all three independent translational directions,  $k_x$  (red),  $k_y$  (blue), and  $k_z$  (green) are shown. Lines are drawn with slopes of 2 and 3.

For small particle sizes ( $r < 50$  nm), the trap stiffness is proportional to  $r^3$ , whereas for larger particles, the increase in  $k$  with  $r$  is less steep. This is in accordance with the fact that the gradient force is proportional to volume as long as the particle radius is on the order of, or smaller than, the skin depth. For larger particles, only a shell is polarized, hence, the increase in  $k$  versus  $r$  is slower. If the polarized part of the particle could be considered a true shell, the increase would be assumed to increase as  $r^2$ . However, as can be seen from Figure 3, the increase for larger particles appears more slowly than that of  $r^2$ . Note that for particles with  $r = 75$  nm, the spring constant was a bit below the value expected (following the tendency from both the smaller and larger particles). This is in accordance with our earlier experience with trapping gold nanoparticles,<sup>3</sup> where this size of particles was simply more difficult to stably trap than sizes smaller or larger. For all particle sizes, the lateral direction designated “y”, parallel to the polarization of the laser light, was strongest. The other lateral direction,  $x$ , was consistently weaker than the  $y$  direction. For the smallest particle size that could be stably trapped ( $r = 10$  nm), data was not of a sufficient quality to perform a reliable estimate of  $k_z$ . However, for the larger particle sizes, it is noticeable that  $k_z$  increases more slowly with particle size than  $k_x$  and  $k_y$  do. The larger the particle, the weaker the trap was in the axial direction in comparison to its lateral strength. This is probably because the increased particle size renders an increased scattering force, which tends to destabilize the trap in the axial direction.

Similar data, showing the relation between trap stiffness and particle radius, taken using the oil immersion objective is shown in Figure 4. Many of the same conclusions reached for the data taken by the water immersion objective also hold true for the data from the oil immersion objective. However, there are some differences: using the oil immersion objective with the optimized immersion oil gives data for the smallest particles ( $r = 10$  nm) that are of a significantly better quality than the water immersion does, e.g., it is possible to perform a quantitative analysis of the axial strength,  $k_z$ , for the smallest particle size. By comparing Figures 3 and 4, it is clear that the axial strength using the oil immersion objective

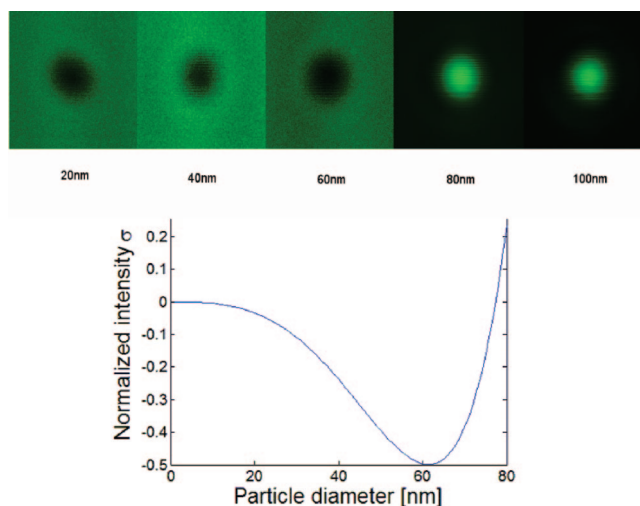


**Figure 5.** Upper panel shows images of silver nanoparticles at the glass water interface obtained by confocal reflection microscopy. The graph shows the normalized intensity of the center of the spot,  $\sigma$  from eq 5, as a function of particle diameter.

is as strong as using the water immersion objective. This is in contrast to previous results of trapping gold nanoparticles,<sup>3</sup> where the oil immersion objective created a significantly weaker trap than the water immersion objective did. Also, the axial strength increases with particle size in the same manner as the lateral directions do, not slower as was the case for the data taken by the water immersion objective. This probably indicates that using the oil immersion objective together with an optimized immersion oil gives a stronger and more stable optical trap for all particle sizes, in particular in the axial direction, than using a water immersion objective. As with the water immersion objective, we see a pronounced dip in trap performance in all directions for particles with sizes around  $r = 75$  nm using the oil immersion objective.

We find that the smallest particles ( $r = 10$  nm) are difficult to maintain trapped. This is supported by previous results using gold nanoparticles, where particles of size  $r = 6$  nm could not be trapped by laser powers as high as 800 mW.<sup>3</sup> As evident from eq 1, the gradient force exerted on nanoparticles scales linearly with polarizability and thus with the polarized volume of the particle. For particles with radii smaller than the skin depth, as is the case for typical Rayleigh particles, the entire volume is polarized and the gradient force scales directly with the volume of the particle. Metallic particles with diameters smaller than around 20 nm require extremely high laser powers, e.g., pulsed lasers, to create a potential deeper than the thermal energy ( $K_B T$ ).<sup>3</sup> However, metallic nanoparticles larger than 20 nm can be trapped by long wavelength light. Interestingly, on the basis of our experience from optical trapping of silver and gold nanoparticles, the smallest nanoparticles are more stably trapped if composed of gold rather than silver. This is consistent with the numerical predictions of ref 11 that gold is more stably trapped at long trapping wavelengths, while silver is trapped better at short wavelengths.

By using a confocal microscope in reflection mode, we were able to visualize all optically trapped silver nanopar-

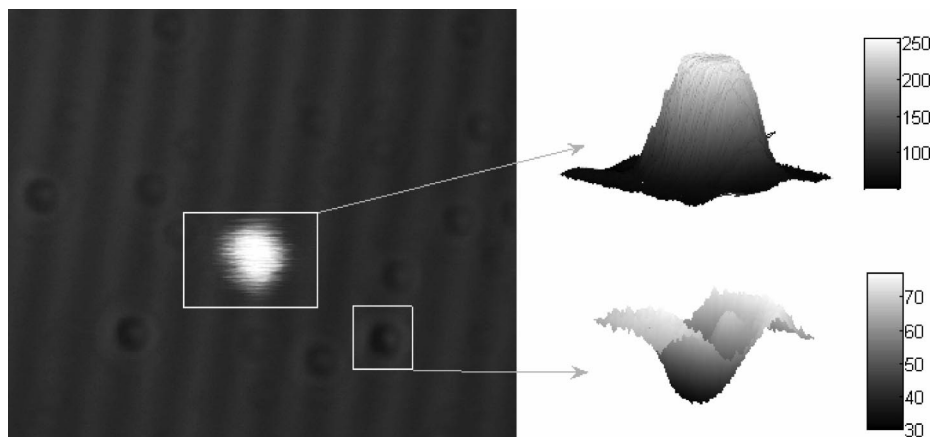


**Figure 6.** A 60 nm particle held by an optical trap (bright spot) above the surface, similar particles attached to the surface are visible as dark spots slightly out of focus. Right: surface plots of the trapped and surface adhered particles showing the magnitude of the signal compared to the background.

ticles. Figure 5 shows images of the smallest particle sizes adhered to a glass cover slip. The particles are smaller than the optical resolution, and consequently, what is seen is the point spread function of the microscope. The measured light from the position of the particle originated from the particle and the glass surface, respectively, but also from the interference between the two.

This change of reflected intensity,  $I_m$ , from the scanning laser has the form<sup>9</sup>

$$I_m \propto r^2 + s^2 - 2r|s|\sin\phi \quad (4)$$

where  $r$  is the background reflected light predominantly from the glass/water interface and  $s$  is the complex scattering amplitude from the particle with phase  $\phi$ . For very small particles, the first term dominates and only the background is visible. For larger particles, the third term, which is negative and goes as  $d^3$ , dominates and the spot appears dark in comparison to the background. For even larger particles, the second term, which is positive and goes as  $d^6$ , dominates and the spot appears bright. Figure 5 shows a plot of the normalized intensity

$$\sigma = \frac{I_m - I_r}{I_r} \quad (5)$$

as a function of particle size.  $I_r$  is the background intensity. This behavior described above is clearly observed in Figure 5, where the center of the image changes from dark to bright in comparison to the background for particle diameters between 60 and 80 nm. Similar behavior has been reported for gold nanoparticles,<sup>9,10</sup> but this is the first time it has been shown to hold true for silver as well. The wavelength used for visualization of the silver nanoparticles was 488 nm, this wavelength being above the plasmon resonance wavelength of silver. The size at which the scattering term begins to dominate the negative interference term in eq 4 is when the diameter is  $\sim 70$  nm. This crossover might be a result of more pronounced retardation effects as the size of the particle increases. We note that the size of particle where this crossover takes place is smaller than the size of the particles (diameter  $\sim 140$  nm), which for some still unknown reason are more difficult to trap than the larger and smaller particles.

Figure 6 shows a 60 nm silver particle held in an optical trap approximately  $5 \mu\text{m}$  above the surface. The particle in

the trap appears bright, whereas the particles, which are of similar size but adsorbed to the surface, appear dark due to the stronger background reflectivity at the surface (in accordance with Figure 5). Confocal imaging of a trapped particle as shown in Figure 6 is relatively slow compared to its rapid Brownian motion. Therefore, the image reflects the range of positions visited by the particle. The focus of the objective coincided with the position of the optical trap.

We report stable three-dimensional optical trapping of individual silver nanoparticles with diameters between 20 and 275 nm. Quantitative analysis of the optical trapping strength shows that the larger the particle, the stronger the optical trap. Optimizing the optical trap created by an oil immersion objective, resulted in an exceptionally strong trap, the axial strength of which was equal to its lateral strength. Thus, in contrast to previous studies, for the smallest particles, the trap formed by an oil immersion objective performed better than a trap based on a water immersion objective. For particles with diameters smaller than 150 nm, the trapping strength was proportional to volume, however, for larger particles, the strength increased even slower than  $r^2$ . We did not find an upper size limit, and we were only limited by which silver nanoparticles were commercially available in a sufficient quality. As the potential depth of the trap for a particle 20 nm in diameter is on the order of a few  $k_B T$ , it is unlikely that much smaller particles are trappable. We performed a confocal visualization of silver nanoparticles; in comparison to the background, the smallest particles appeared dark in the central region, but for particles larger than 60 nm, there was a profound crossover, those appearing bright in the central region. Gold nanoparticles have the disadvantage that they quench fluorescence. In contrast, silver nanoparticles are known to considerably enhance fluorescence of specific fluorophores. Therefore, silver nanoparticles are obvious choices as handles of fluorescent nanoscale systems, and we have demonstrated that optical manipulation of individual silver nanoparticles is indeed possible and considerable optical forces can be exerted on them.

**Acknowledgment.** We acknowledge discussions with S. N. S. Reihani and A. C. Richardson as well as using the on-line calibration Labview program created by S. N. S.

Reihani. This work was supported by the Villum Kann Rasmussens Foundation through BioNET.

## References

- (1) Aslan, K.; Lakowicz, J. R.; Geddes, C. D. *Anal. Bioanal. Chem.* **2005**, *382*, 926–933.
- (2) Svoboda, K.; Block, S. M. *Opt. Lett.* **1994**, *19*, 930–932.
- (3) Hansen, P. M.; Bhatia, V. K.; Oddershede, L. *Nano Lett.* **2005**, *5*, 1937–1942.
- (4) Sepulveda, B.; Alegret, J.; Käll, M. *Opt. Express* **2007**, *15*, 14914–14920.
- (5) Prikulis, J.; Svedberg, F.; Goksör, M.; Hanstorp, D. *Nano Lett.* **2004**, *4*, 115–118.
- (6) Yoshikawa, H.; Adachi, T.; Sazaki, G.; Matsui, T.; Nakajima, K.; Masuhara, H. *J. Opt. A: Pure Appl. Opt.* **2007**, *9*, S164–S171.
- (7) Seol, Y.; Carpenter, A. E.; Perkins, T. T. *Opt. Lett.* **2006**, *31*, 2429–2431.
- (8) Reihani, S. N. S.; Oddershede, L. *Opt. Lett.* **2007**, *32*, 1998–2000.
- (9) Lindfors, K.; Kalkbrenner, T.; Stoller, P.; Sandoghdar, V. *Phys. Rev. Lett.* **2004**, *93*, 037401-1–037401-4.
- (10) Jacobsen, V.; Stoller, P.; Brunner, C.; Vogel, V.; Sandoghdar, V. *Opt. Express* **2006**, *14*, 405–414.
- (11) Quidant, R.; Zelenina, A. S.; Nieto-Vesperinas, M. *Appl. Phys. A: Mater. Sci. Process.* **2007**, *89*, 233–239.
- (12) Oddershede, L.; Grego, S.; Nørrelykke, S. F.; Berg-Sørensen, K. *Probe Microsc.* **2001**, *2*, 129–137.
- (13) Richardson, A. C.; Oddershede, L. B. *SPIE Proc.* **2007**, *6326*, 28–38.
- (14) Arias-Gonzalez, J. R.; Vieto-Vesperinas, M. *J. Opt. Soc. Am. A* **2003**, *20*, 1201–1209.
- (15) Rohrbach, A. *Phys. Rev. Lett.* **2005**, *95*, 168102-1–168102-4.
- (16) Hansen, P. M.; Tolic-Nørrelykke, I. M.; Flyvbjerg, H.; Berg-Sørensen, K. *Comput. Phys. Commun.* **2006**, *174*, 518–520.
- (17) Berg-Sørensen, K.; Oddershede, L.; Florin, E.-L.; Flyvbjerg, H. *J. Appl. Phys.* **2003**, *93*, 3167–3177.
- (18) Dreyer, J. K.; Berg-Sørensen, K.; Oddershede, L. *Appl. Opt.* **2004**, *43*, 1991–1996.

NL080490+